Research Article

Conjugate heat transfer performance of stepped lid-driven cavity with Al$_2$O$_3$/water nanofluid under forced and mixed convection

Naveen Janjanam[1] · Rajesh Nimmagadda[1,2] · Lazarus Godson Asirvatham[3] · R. Harish[4] · Somchai Wongwises[5,6]

Abstract

Two-dimensional conjugate heat transfer performance of stepped lid-driven cavity was numerically investigated in the present study under forced and mixed convection in laminar regime. Pure water and Aluminium oxide (Al$_2$O$_3$)/water nanofluid with three different nanoparticle volume concentrations were considered. All the numerical simulations were performed in ANSYS FLUENT using homogeneous heat transfer model for Reynolds number, Re = 100 to 500 and Grashof number, Gr = 5000, 13,000 and 20,000. Effective thermal conductivity of the Al$_2$O$_3$/water nanofluid was evaluated by considering the Brownian motion of nanoparticles which results in 20.56% higher value for 3 vol.% Al$_2$O$_3$/water nanofluid in comparison with the lowest thermal conductivity value obtained in the present study. A solid region made up of silicon is present underneath the fluid region of the cavity in three geometrical configurations (forward step, backward step and no step) which results in conjugate heat transfer. For higher Re values (Re = 500), no much difference in the average Nusselt number (Nu$_{avg}$) is observed between forced and mixed convection. Whereas, for Re = 100 and Gr = 20,000, Nu$_{avg}$ value of mixed convection is 24% higher than that of forced convection. Out of all the three configurations, at Re = 100, forward step with mixed convection results in higher heat transfer performance as the obtained interface temperature is lower than all other cases. Moreover, at Re = 500, 3 vol.% Al$_2$O$_3$/water nanofluid enhances the heat transfer performance by 23.63% in comparison with pure water for mixed convection with Gr = 20,000 in forward step.

Keywords Conjugate · Stepped · Lid-driven · Numerical · Brownian motion · Nusselt number

Abbreviations

c	Constant	L	Length (m)
C_p	Specific heat (J/kg K)	M	Molecular weight (kg/kmole)
D	Diameter (m)	n	Empirical shape factor
g	Acceleration due to gravity (m/sec^2)	Nu	Nusselt number
Gr	Grashof number	P	Pressure (kg/m sec^2)
h	Convective heat transfer coefficient (W/m^2 K)	Pr	Prandtl number
k	Thermal conductivity (W/m K)	q	Heat flux (W/m^2)
k_m	Matrix thermal conductivity (W/m K)	R	Thermal boundary resistance coefficient (K m^2/W)
K_B	Boltzmann constant (J/K)	Re	Reynolds number
		t	Time (sec)

✉ Rajesh Nimmagadda, rajesh.mech335@gmail.com | [1]Department of Mechanical Engineering, Koneru Lakshmaiah Educational Foundation, Vaddeswaram, Andra Pradesh (A.P), India. [2]Center for Advanced Energy Studies, Koneru Lakshmaiah Educational Foundation, Vaddeswaram, Andra Pradesh (A.P), India. [3]Department of Mechanical Engineering, Karunya Institute of Technology and Sciences, Coimbatore, Tamil Nadu (T.N), India. [4]Thermal and Automotive Division, School of Mechanical Engineering, Vellore Institute of Technology, Chennai, Tamil Nadu (T.N), India. [5]Department of Mechanical Engineering, Faculty of Engineering, King Mongkut's University of Technology Thonburi, Bangkmod, Bangkok, Thailand. [6]National Science and Technology Development Agency (NSTDA), Pathum Thani, Thailand.

T Temperature (K)
$\vec{U}$ Velocity vector (m/sec)
U Horizontal velocity (m/sec)
V Vertical velocity (m/sec)
X Horizontal coordinate
Y Vertical coordinate

Greek symbols
β Coefficient of thermal expansion (1/K)
δ Index coefficient
μ Dynamic viscosity (kg/m sec)
v Kinematic viscosity (m^2/sec)
ϕ Volume concentration
ρ Density (kg/m^3

Subscripts
avg   Average
bf   Base fluid
bw   Thermal boundary resistance of water
c   Cluster
f   Fluid
h   High
l   Low
nf   Nanofluid
p   Particle
s   Solid

1 Introduction

Rapid growth in the usage of high-performance electronic devices with compact size requires efficient cooling systems [1, 2]. Apart from this, the system should also be capable of preventing the leakage associated with the circulating coolant. This leakage problem will be well eliminated when one switches to closed cooling system rather than the open type [3]. This is because the circulating coolant will never leave the system there by causing no leakage into the surrounding electronic circuits. Moreover, efficient coolants are also essentially needed when compared with conventional heat transfer fluids so that the large quantities of heat generated from the electronic devices can be easily dissipated. Dispersing nanoparticles within the conventional heat transfer fluids such as water or ethylene glycol will enhance the effective thermal conductivity of the coolant thereby enhancing the heat transfer performance of the cooling system. These coolants with nanoparticles are named as "nanofluids," and they have wide variety of applications [4, 5].

Many classical thermal conductivity models were developed in eighteenth and nineteenth centuries for predicting the effective thermal conductivity of solid–liquid mixtures. Maxwell [6] developed a static thermal conductivity model for mixtures with low volume concentration of spherical particles. This model fails when the concentration of particles is sufficiently higher. This failure is avoided by the thermal conductivity model developed by Bruggeman [7], which can be applied even to high volume concentration of nanoparticles which are of spherical shape. The particle shape, size and particle interactions for thermal conductivity evaluation were not considered in these models. Hamilton and Crosser [8] moved a step higher by developing a thermal conductivity model with inclusion of particle shape by introducing empirical shape factor (n). Lu and Lin [9] thermal conductivity model consider pair interactions that is obtained by solving a boundary value problem. Chon et al. [10] took nanoparticle diameter into consideration and developed an experimental thermal conductivity correlation for Al$_2$O$_3$/water nanofluids. Experimental investigation along with theoretical determination of thermal conductivity of Al$_2$O$_3$/water nanofluid was carried out by Chandrasekar et al. [11]. Khanafer and Vafai [12] observed that the obtained experimental results reported by several researchers for the effective thermal conductivity disagree and requirement of additional experimental and theoretical research studies is very essential in order to clarify the mechanisms responsible for nanofluid heat transfer enhancement.

Xuan et al. [13] developed a theoretical model to predict the thermal conductivity of nanofluids by considering properties of nanoparticles and base fluid, as well as the structure of the nanoparticles and aggregates. Patel et al. [14] developed thermal conductivity model for nanofluids by considering micro-convection phenomena involving Brownian motion as well as increment in the specific area. The developed thermal conductivity model will give good insight on phenomena involved at nanoscale. According to the observations of Prasher et al. [15], no concrete conclusions have been reached among various thermal conductivity models and mechanisms proposed in the literature. He concluded that Brownian motion is mainly responsible for nanofluid thermal conductivity enhancement. Incorporation of Brownian motion into the thermal conductivity model along with particle size was carried out by Dong and Chen [16]. Goudarzi et al. [17] numerically investigated migration of nanoparticles under Brownian diffusion and concludes it as an important enhancing phenomenon in heat transfer. Abdelmalek et al. [18] as well as Harish and Sivakumar [19] observed that both the effects of thermophoresis and Brownian motion surges the thermal energy of fluid and are significantly important. Higher heat transfer enhancement is observed with the use of Maxwell model when compared with that of traditional model in the numerical investigation carried out by Lin and Jiang [20].

Gibanov et al. [21, 22] carried out numerical investigation on ferro fluid and alumina nanofluid mixed convection

in a lid-driven cavity with backward step heat conducting solid region. The observations proved that the sizes and conductivity of the backward step will essentially change both the flow behavior as well as heat transfer patterns. Numerical study has been carried out by Al-Amiri et al. [23] on lid-driven cavity with a sinusoidal wavy bottom surface for analyzing the mixed convection heat transfer. It is observed from the study that by increasing the amplitude of the wavy surface and Reynolds number, the average Nusselt number increases. Khanafer and Aithal [24] also investigated mixed convection heat transfer flow phenomena in a lid-driven cavity fitted with a circular body. The study reported that by placing cylinder near the bottom wall of the cavity, an optimal heat transfer performance is obtained. Mixed convection in lid driven cavity with heated triangular block is numerically studied by Gangawane [25]. The study concluded that the convection heat transfer can be controlled by inserting triangular body into the lid-driven cavity. Khan et al. [26] numerically observed that heat transfer rate in a split lid-driven cavity enhances by placing a Y-shaped obstacle. Unsteady mixed convection in lid-driven enclosure with oscillatory walls was numerically investigated by Valizadeh Ardalan et al. [27] by using Cu/water nanofluid. The study concluded that reduction in the frequency of wall oscillation leads to enhancement in the heat transfer.

However, from the above-mentioned literature [12, 15], it can be observed that no concrete conclusions have been reached among various thermal conductivity models and mechanisms proposed in the literature. Moreover, as per [14], the thermal conductivity model needs to consider micro-convection phenomena involving Brownian motion. This is the reason, in the present study, various thermal conductivity models were used for the comparison of the effective thermal conductivity of Al_2O_3/water nanofluid for different nanoparticle volume concentration. Moreover, in the present study for numerical simulations with Al_2O_3/water nanofluid the effective thermal conductivity model

of [14] is used, as this model takes into consideration; the brownian motion effect of nanoparticles. Furthermore, as mentioned in the literature [21–23], it can be understood that the sizes and conductivity of the backward step essentially change both the flow and heat transfer patterns in mixed convection. This is the reason, in the present study, a solid region made up of silicon is present underneath the fluid region of the lid-driven cavity in three geometrical configurations (forward step, backward step and no step) results in conjugate heat transfer. Pure water and Al_2O_3/water nanofluid with three different nanoparticle volume concentrations were considered. All the numerical simulations were performed using homogeneous heat transfer model in ANSYS FLUENT. The effect of various parameters such as Reynolds number (Re = 100 to 500), Grashof number (Gr = 5000, 13,000 and 20,000), geometrical configuration, convection types are comprehensively investigated and presented.

2 Geometry description

Conjugate heat transfer performance of stepped lid-driven cavity was numerically investigated in the present study under forced and mixed convection. The flow is assumed to be two dimensional and in laminar regime. As observed in Fig. 1a–c, solid region made up of silicon is considered underneath the fluid region of the cavity in three geometrical configurations (forward step, backward step and no step) resulting in conjugate heat transfer. The reason for using silicon is because; it is most commonly and widely used semiconductor material in electronic devices. The properties of silicon such as thermal conductivity, specific heat and density are chosen to be 149 W/m K, 710 J/kg K and 2329 kg/m^3, respectively. The length (L) of the cavity is chosen to be 0.005 m. This length scale is selected in such as way that it is suitable for general electronic devices especially for micro processors as available in today's market. Pure water and
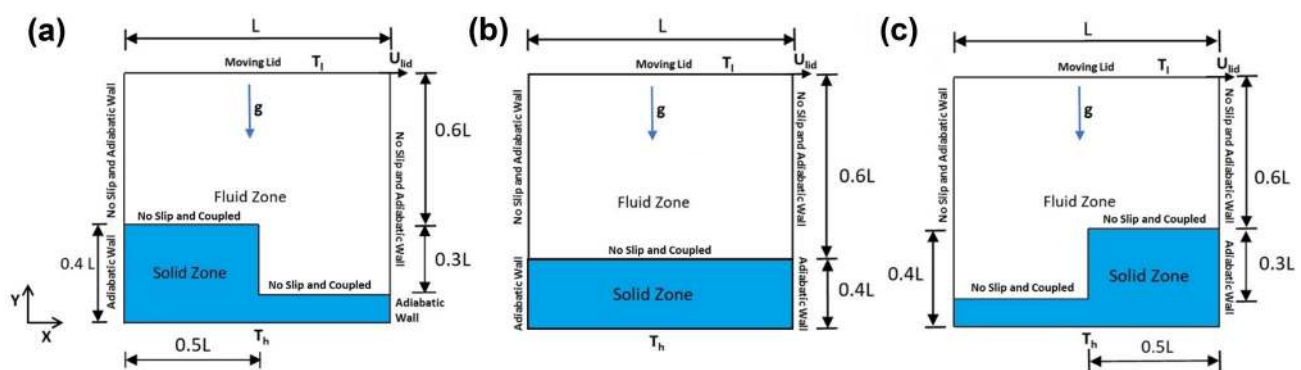

Fig. 1 Schematic representation of the cavity in three geometrical configurations: **a** Forward step, **b** No step and **c** Backward step

Al$_2$O$_3$/water nanofluid with 1, 2 and 3 vol.% concentrations with a particle diameter (D_p) of 30 nm were considered in the present study. The lid at the top of the cavity moves in horizontal direction with a velocity (U_{lid}) whose magnitude is given in the form of a dimensionless number called as Reynolds number (Re). All the numerical simulations were performed using homogeneous heat transfer model in ANSYS FLUENT for Re = 100 to 500 and Gr = 5000, 13,000 and 20,000.

3 Thermophysical properties

The properties of Al$_2$O$_3$/water nanofluid such as density, specific heat and thermal expansion coefficient are evaluated in the present study using Eqs. 1–3 that are based on mixture theory. These equations are also used in Pak and Cho [28], Xuan and Roetzel [29] as well as Nimmagadda [30], respectively. The nanofluid dynamic viscosity was evaluated by using the Brinkman equation [31] and the nanofluid effective thermal conductivity was evaluated from the model developed by Patel et al. [14]. Patel et al. [14] model takes in to account the Brownian velocity of nanoparticles within the base fluid. The properties of nanoparticles as well as base fluid used in the present study are adopted from Ho et al. [32] summarized in Table 1. The below given equations were used in the evaluation of the thermophysical properties.

$$\rho_{nf} = \phi\rho_p + (1-\phi)\rho_{bf} \tag{1}$$

$$(\rho C_P)_{nf} = \phi(\rho C_P)_p + (1-\phi)(\rho C_P)_{bf} \tag{2}$$

$$(\rho\beta)_{nf} = \phi(\rho\beta)_p + (1-\phi)(\rho\beta)_{bf} \tag{3}$$

$$\mu_{nf} = \frac{\mu_{bf}}{(1-\phi)^{2.5}} \tag{4}$$

$$\frac{k_{nf} - k_{bf}}{k_{bf}} = \frac{k_p}{k_{bf}}\left(1 + c\frac{u_p D_p}{\alpha_{bf}}\right)\frac{D_{bf}}{D_p}\frac{\phi}{(1-\phi)} \tag{5}$$

Here, $c = 25{,}000$, value obtained from extensive experimental results and $D_{bf} = 2.75 \times 10^{-10}$ m.

u_p is Brownian velocity of nanoparticles and it is given by the formula, $u_p = \frac{2K_B T}{\pi\mu_{bf}D_p^2}$. Here, T indicates the initial tem-

perature of nanofluid, and its value is chosen to be 303 K which indicates the atmospheric temperature. Patel et al. [14] model is also compared with various thermal conductivity models available in the literature with and without consideration of Brownian motion. All the thermal conductivity models used in the comparison are given in Table 2.

4 Mathematical representation

Two-dimensional conjugate heat transfer performance of stepped lid-driven cavity was numerically investigated in the present study under forced and mixed convection in laminar regime. All the numerical simulations were performed using homogeneous heat transfer model in ANSYS FLUENT for Reynolds number, Re = 100 to 500 and Grashof number, Gr = 5000, 13,000 and 20,000. The governing equations, boundary conditions and Nusselt number evaluation that were implemented in the present study are given in the below sections.

4.1 Governing equations

Homogeneous heat transfer model based on Finite Volume Method (FVM) formulation for steady state incompressible two-dimensional laminar flow with in ANSYS FLUENT is used in the present study. For single phase flow problems this particular model is used. However, nanofluids in which dispersed nanoparticles were present are treated as homogeneous mixture in the present study whose thermophysical properties are evaluated as in section with the use of well-established correlations. The obtained properties of nanofluids are used in the homogeneous heat transfer model applicable for single phase flows for evaluation. The steady state equations for velocity and temperature fields are as follows [33, 34].

Equation for conservation of mass

$$\nabla \cdot \left(\rho_{nf}\vec{U}\right) = 0 \tag{6}$$

Equation for conservation of momentum

$$\nabla \cdot \left(\rho_{nf}\vec{U}\vec{U}\right) = -\nabla p + \mu_{nf}\nabla^2\vec{U} + (\rho\beta)_{nf}g\left(T_{nf} - T_l\right) \tag{7}$$

The third term on the right-hand side of the above momentum equation is the buoyancy term which takes in to account the effect of natural convection. This term represents the buoyancy force acting on the fluid as a result of the temperature difference. T_l in the buoyancy term represents the low temperature at which the top horizontal wall of the cavity is maintained, and its value is chosen to be 303 K in the present study. For mixed convection flows,

Table 1 Base fluid and nanoparticle properties adopted from Ho et al. [32]

Fluid/Nanoparticle	Properties			
	$\rho\left\lvert\frac{kg}{m^3}\right.$	$C_p\left\lvert\frac{J}{Kg\,K}\right.$	$\mu\left\lvert\frac{Kg}{m\,sec}\right.$	$kK\left\lvert\frac{W}{m\,K}\right.$
Pure water	995.1	4178	0.00083	0.62
Al$_2$O$_3$	3600	765	–	36

Table 2 Thermal conductivity models used for comparison as shown in Fig. 8

Researcher	Thermal conductivity model
Maxwell [6]	$k_{nf} = \frac{k_p + 2k_{bf} + 2\phi(k_p - k_{bf})}{k_p + 2k_{bf} - \phi(k_p - k_{bf})} k_{bf}$
Bruggeman [7]	$\frac{k_{nf}}{k_{bf}} = \frac{(3\phi-1)\frac{k_p}{k_{bf}} + [3(1-\phi)-1] + \sqrt{\left\{(3\phi-1)\frac{k_p}{k_{bf}} + [3(1-\phi)-1]\right\}^2 + 8\frac{k_p}{k_{bf}}}}{4}$
Hamilton and Crosser [8]	$k_{nf} = \frac{k_p + (n-1)k_{bf} - (n-1)(k_{bf} - k_p)\phi}{k_p + (n-1)k_{bf} + (k_{bf} - k_p)\phi} k_{bf}$
Lu and Lin [9]	$k_{nf} = \left(1 + 3\phi + 4.5\phi^2\right) k_{bf}$
Chon et al. [10]	$\frac{k_{nf}}{k_{bf}} = 1 + 64.7\phi^{0.746}\left(\frac{D_{bf}}{D_p}\right)^{0.369}\left(\frac{k_p}{k_{bf}}\right)^{0.7476} Pr^{0.9955} Re^{1.2321}$
Chandrasekar et al. [11]	$\frac{k_{nf}}{k_{bf}} = \left(\frac{C_{p_{nf}}}{C_{p_{bf}}}\right)^{-0.023}\left(\frac{\rho_{nf}}{\rho_{bf}}\right)^{1.358}\left(\frac{M_{bf}}{M_{nf}}\right)^{0.126}$
Khanafer and Vafai [12]	$\frac{k_{nf}}{k_{bf}} = 1.0 + 1.0112\phi + 2.4375\phi\left(\frac{47}{D_p innm}\right) - 0.0248\phi\left(\frac{k_p}{0.613}\right)$
Xuan et al. [13]	$\frac{k_{nf}}{k_{bf}} = \frac{k_p + 2k_{bf} - 2\phi(k_{bf} - k_p)}{k_p + 2k_{bf} + \phi(k_{bf} - k_p)} + \frac{\rho_p \phi C_p}{2k_{bf}}\sqrt{\frac{K_B T}{3\pi r_c \mu_{bf}}}$
Patel et al. [14]	$\frac{k_{nf} - k_{bf}}{k_{bf}} = \frac{k_p}{k_{bf}}\left(1 + c\frac{u_p D_p}{\alpha_{bf}}\right)\frac{D_{bf}}{D_p}\frac{\phi}{(1-\phi)},$ Here, $u_p = \frac{2K_B T}{\pi \mu_{bf} D_p^2}$
Prasher et al. [15]	$\frac{k_{nf}}{k_{bf}} = \left(1 + ARe^m Pr^{0.333}\phi\right)$ $\times \left[\frac{\left(k_p\left(1 + 2\left(\frac{2R_{bw}k_m}{D_p}\right)\right) + 2k_m\right) + 2\phi\left(k_p\left(1 - \left(\frac{2R_{bw}k_m}{D_p}\right)\right) - k_m\right)}{\left(k_p\left(1 + 2\left(\frac{2R_{bw}k_m}{D_p}\right)\right) + 2k_m\right) - \phi\left(k_p\left(1 - \left(\frac{2R_{bw}k_m}{D_p}\right)\right) - k_m\right)}\right]$ Here, for water-based nanofluids, $A = 4 \times 10^4$, $m = 2.5 \pm 15\%$ $k_m = k_{bf}\left[1 + \left(\frac{1}{4}RePr\right)\right]$ and $Re = \frac{1}{\nu}\sqrt{\frac{18K_B T}{\pi \rho_p D_p}}$
Dong and Chen [16]	$k_{nf} = \frac{(\delta+1)k_{bf} + \delta k_p + 2\delta\phi(k_p - k_{bf})}{(\delta+1)k_{bf} + \delta k_p - \delta\phi(k_p - k_{bf})} k_{bf}$

this buoyancy term will be activated. Whereas, for forced convection flows, it will be neglected.

Equation for conservation of energy in fluid zone

$$\nabla \cdot \left(\left(\rho C_p\right)_{nf} \vec{U} T_{nf}\right) = \nabla \cdot \left(k_{nf} \nabla T_{nf}\right) \tag{8}$$

Energy equation for solid zone

$$\nabla^2 T_s = 0 \tag{9}$$

The three dimensionless numbers presented in the numerical investigation are Reynolds number (Re), Grashof number (Gr) and Nusselt number. Reynolds number is the ratio of inertia force to viscous force and is given as follows.

$$Re = \frac{\rho_f U_{lid} L}{\mu_f} \tag{10}$$

whereas, Grashof number is defined as the ratio of buoyancy force to viscous force acting on fluid and is given as follows.

$$Gr = \frac{\rho_f g \beta_f (T_h - T_l) L^3}{\mu_f^2} \tag{11}$$

T_h in the above equation represents the high temperature at which the bottom wall of the solid region is maintained, and its value is obtained from Grashof number.

Whereas, Nusselt number is defined as the ratio of convection heat transfer to fluid conduction heat transfer. The average Nusselt number adopted in the present study is given as follows.

$$Nu_{avg} = \frac{h_{interface_{avg}} L}{k_{bf}} \tag{12}$$

4.2 Boundary conditions

Appropriate boundary conditions are implemented on all the three geometrical lid-driven cavity configurations in the present study. Top wall of the cavity is assigned with a horizontal velocity value obtained from respective Reynolds number. Whereas, the vertical velocity value of it remains zero. No slip velocity boundary condition is implemented on all other walls of the cavity. The top wall of the cavity is maintained at a low temperature (T_l) of 303 K and all the vertical walls are insulated by implementing adiabatic boundary condition with $q = 0$ W/m^2. The bottom wall of the solid region is maintained at a high temperature (T_h) whose value obtained from respective Grashof number. The values of T_h used are 316.51, 338.12 and 357.03 K for Gr = 5000, 13,000 and 20,000, respectively. The interface between solid and fluid zones is implemented with no slip velocity boundary condition and coupled thermal boundary condition. This coupled thermal boundary condition considers that both heat fluxes as well as temperatures of solid and fluid zones at the interface are equal as given by Nimmagadda and Venkatasubbaiah [35].

5 Grid independence test

Grid independence test representing temperature along the solid–fluid interface of the lid-driven cavity in the case of pure water at Re = 100 and Gr = 20,000 in forward step is shown in Fig. 2a. The reason for selecting forward step configuration to conduct grid independence test is because; among all the three configurations used in the present study, forward step configuration showed higher heat transfer performance by exhibiting higher Nu$_{avg}$ values. This test is conducted in order to obtain the optimum grid size beyond which the accuracy of the solution will not alter. As observed in Fig. 2a, four grid sizes: 600 × 600, 800 × 800, 1000 × 1000 and 1200 × 1200 are used in this test. From Fig. 2a, it is clearly observed that the obtained interface temperature is not exhibiting any significant change when the grid size is increased beyond 800 × 800. In this regard, grid size of 800 × 800 is adopted in the present study on all geometrical configurations and on all working parameters. Moreover, the reason for selecting forward step geometrical configuration in this grid independence test is because; this configuration exhibits highest heat transfer performance among all the three geometrical configurations used in the present study. Furthermore, mixed convection at Re = 100 and Gr = 20,000 also exhibits highest heat transfer performance. As all the numerical simulations were performed using homogeneous heat transfer model, pure water is used as heat transfer fluid in this test because there will be no effect of fluid on the gird independence test. Figure 2b represents the grid distribution within the lid-driven cavity at two different locations represented by small square boxes for 800 × 800 grid size. The corresponding enlarged regions of those two small square boxes as shown in Fig. 2b represents that uniform mesh is evenly distributed throughout the computational domain.

6 Model validation

The homogeneous heat transfer model in ANSYS FLUENT used in the present study is validated against the numerical and analytical results available in the literature. To achieve this validation, the geometrical domain and boundary conditions given in the corresponding literature are implemented and solved in ANSYS FLUENT.

Primary validation is done in terms of velocity profiles as shown in Fig. 3a for the case of lid-driven cavity. As observed in Fig. 3a, the horizontal velocity along the vertical height at the center line of the lid-driven cavity is used for comparison. Air at Re = 1000 is used as working fluid inside the cavity and the results obtained with ANSYS FLUENT are compared against the results of Ghia et al. [36] as well as with Mohammed and Reis [37]. From Fig. 3a, the obtained results are in good match with the results of Ghia et al. [36] and that of with Mohammed and Reis [37].

Secondarily, validation is carried out in terms of heat transfer as shown in Fig. 3b for the case of jet impingement. As observed in Fig. 3b, the average Nusselt number values of pure water at various Reynolds number is used for comparison. The results obtained with ANSYS FLUENT are compared against the results of Lamraoui et al. [38] as well as with those of Abhijith and Venkatasubbaiah [39]. From Fig. 3b, the obtained results are in good match with the results of [38] and [39].

After validating the homogeneous heat transfer model in ANSYS FLUENT with the existing results in the literature, the model is then taken into consideration for the present investigation.

7 Results and discussion

Two-dimensional conjugate heat transfer performance of stepped lid-driven cavity was numerically investigated in the present study under forced and mixed convection in laminar regime. Pure water and Aluminium oxide (Al$_2$O$_3$)/water nanofluid with $D_p = 30$ nm and 1 vol.%, 2 vol.% and 3 vol.% concentrations were considered. All these numerical simulations were performed by considering brownian motion based effective thermal

Fig. 2 **a** Grid independence test representing temperature along the solid–fluid interface of the lid-driven cavity in the case of pure water at Re = 100 and Gr = 20,000 in forward step, and **b** Grid distribution within the lid-driven cavity at two different locations represented by small square boxes for 800 × 800 grid size
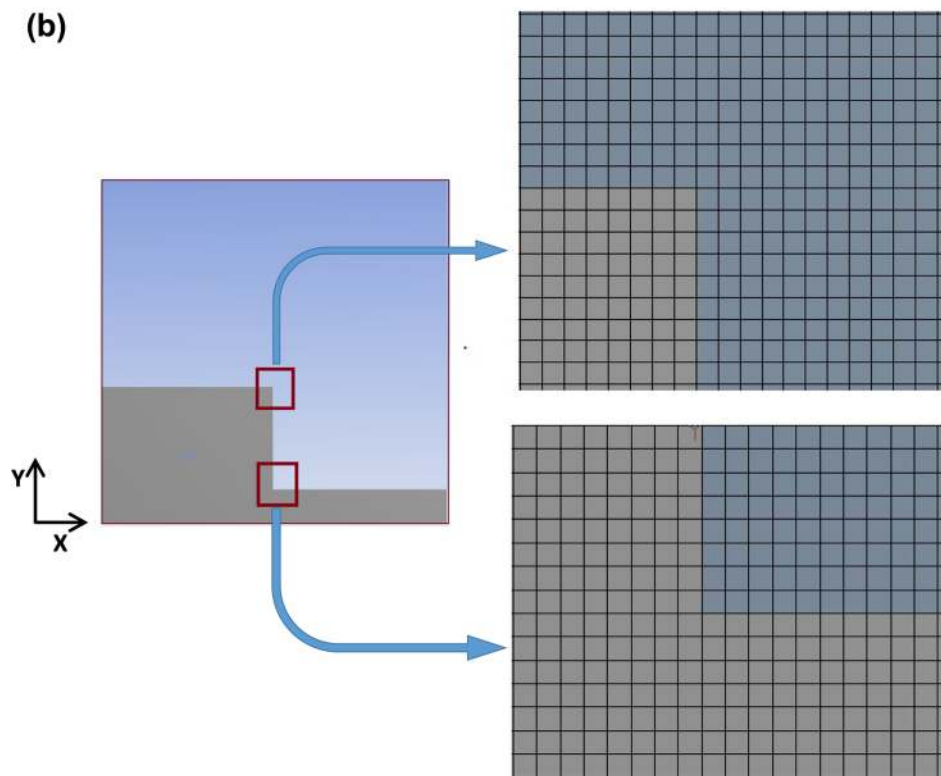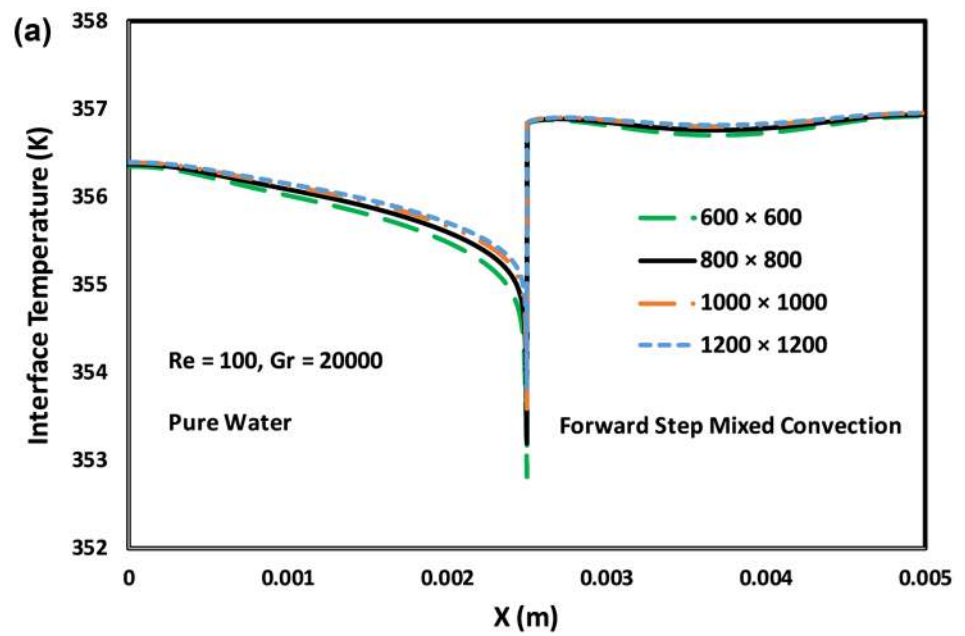
conductivity evaluation in homogeneous heat transfer model of ANSYS FLUENT. The effect of various parameters such as Reynolds number (Re = 100 to 500), Grashof number (Gr = 5000, 13,000 and 20,000), geometrical configuration and convection type are comprehensively investigated and presented.

7.1 Velocity contours

Overlapped X-directional velocity contours of forced and mixed convection in all three geometrical configurations for pure water (colored contour for forced convection and solid black line for mixed convection) at Re = 100 and
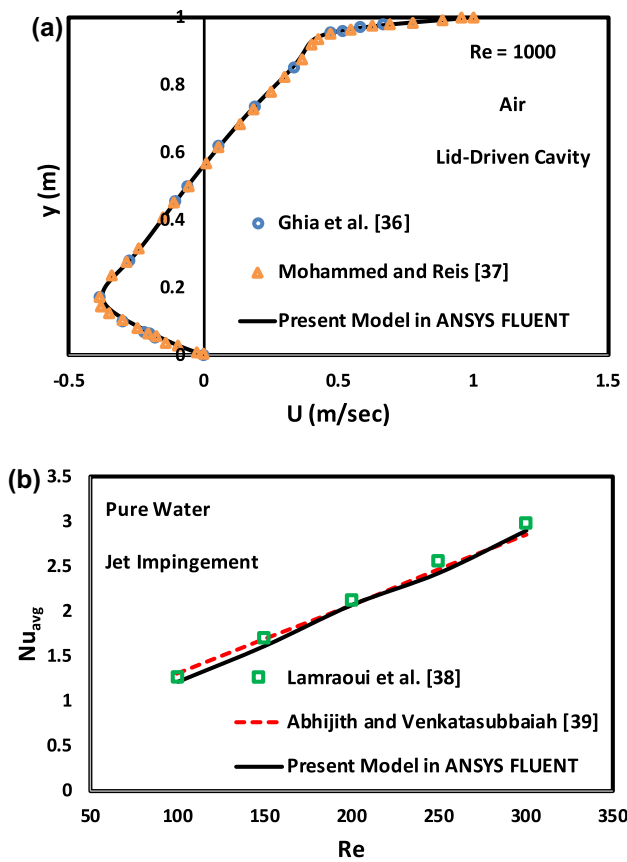
Fig. 3 Velocity and heat transfer validation: **a** Horizontal velocity versus vertical height along the center line of the lid-driven cavity, and **b** Average Nusselt number at different Re for jet impingement

500 are shown in Fig. 4 for Gr = 20,000. From Fig. 4a–c, at Re = 100, it is observed that the colored contour and the solid black line do not overlap with each other resulting in a difference between forced and mixed convection. Whereas, from Fig. 4d–e, at Re = 500, it is observed that the colored contour and the solid black line overlaps with each other. This shows that at higher values of Re, the fluid motion is purely caused by means of external force exerted by moving the lid (by the movement of the lid) and buoyancy effect has very minimal impact on the fluid motion. This is because; the forced currents dominate the tendency of natural fluid movement caused due to difference in local fluid densities which in turn is due to difference in local temperatures. At lower values of Re, domination of forced currents on natural fluid movement is not significant and hence there will be a difference as observed with the mismatch of contours as in Fig. 4a–c.

7.2 Temperature contours

Overlapped temperature contours of forced and mixed convection in all three geometrical configurations for pure water (colored contour for forced convection and solid black line for mixed convection) at Re = 100 and 500 are shown in Fig. 5 for Gr = 20,000. From Fig. 5a–c, at Re = 100, it is observed that the colored contour and the solid black line do not overlap with each other resulting in a difference between forced and mixed convection. Whereas, from Fig. 5d–e, at Re = 500, it is observed that
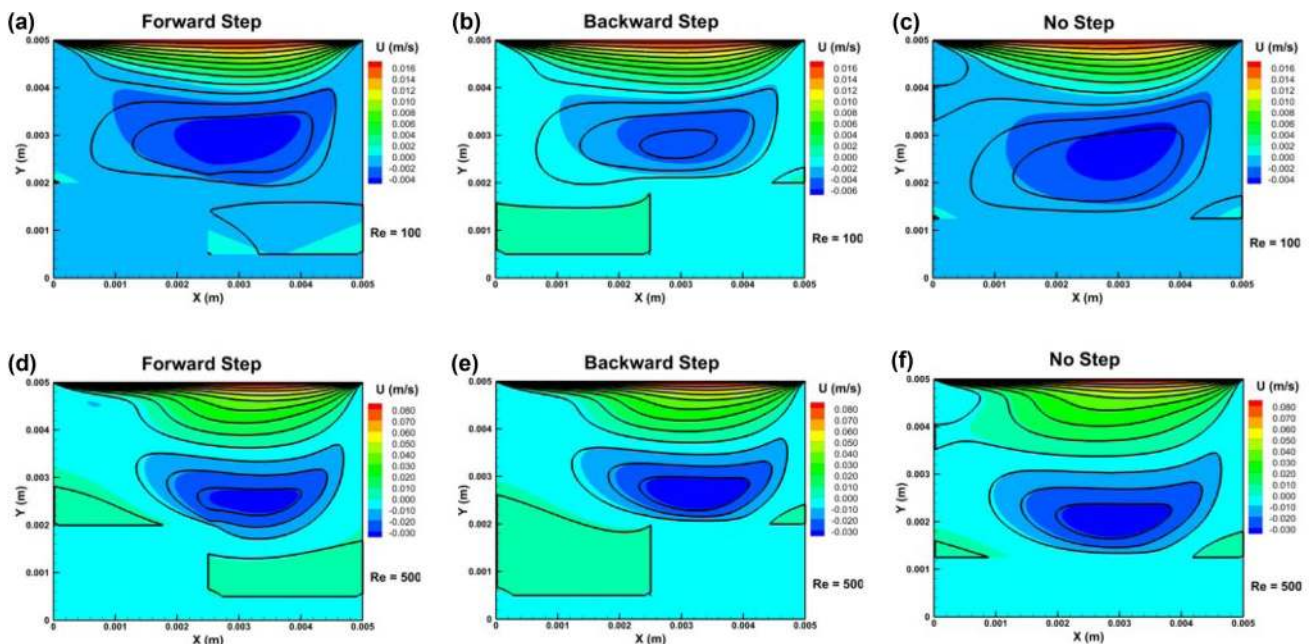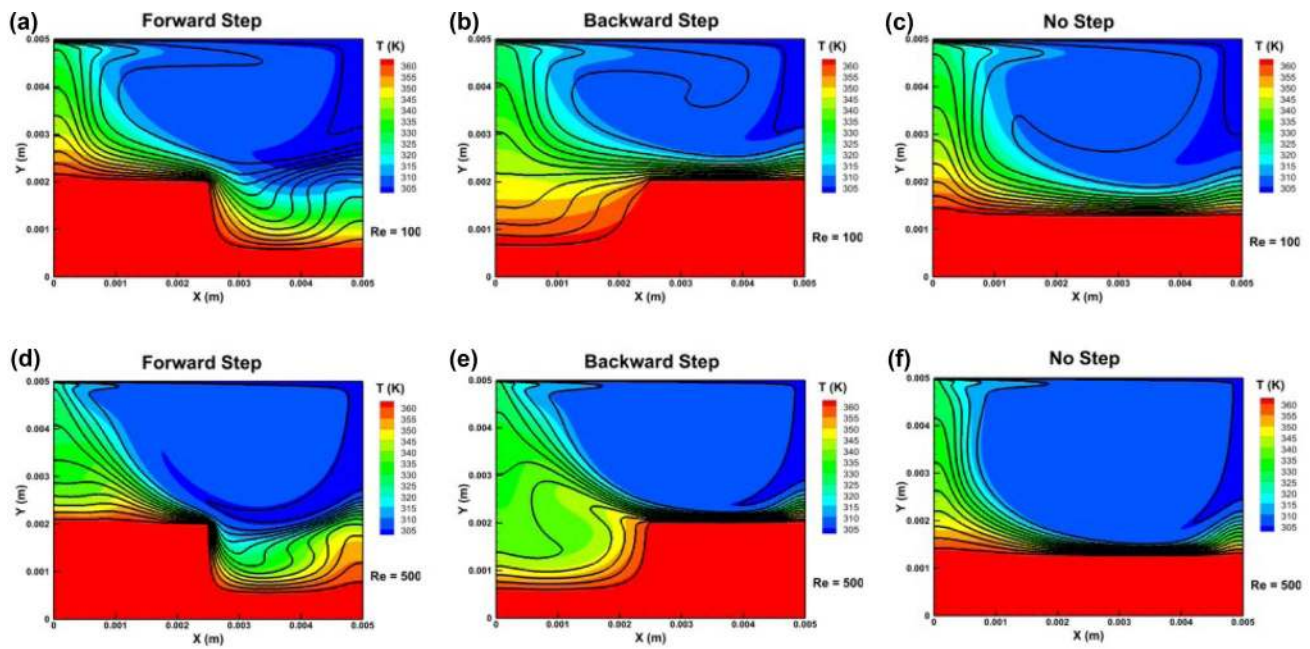

Fig. 4 Overlapped X-directional velocity contours of forced and mixed convection in all three geometrical configurations for pure water (colored contour for forced and solid black line for mixed) at Gr = 20,000: **a** to **c** at Re = 100, **d** to **f** at Re = 500

Fig. 5 Overlapped temperature contours of forced and mixed convection in all three geometrical configurations for pure water (colored contour for forced and solid black line for mixed) at Gr = 20,000: **a** to **c** at Re = 100, **d** to **f** at Re = 500

the colored contour and the solid black line overlaps with each other. As explained in Fig. 5d–e, at higher values of Re, the fluid motion is purely caused by means of external force exerted by the moving lid and buoyancy effect has very minimal impact on the fluid motion. This is because; the forced currents dominate the tendency of natural fluid movement caused due to difference in local fluid densities which in turn is due to difference in local temperatures. At lower values of Re, domination of forced currents on natural fluid movement is not significant and hence there will be a difference as observed with the mismatch of contours as in Fig. 5a–c.

7.3 Effect of geometrical configuration

Temperature distribution present along the solid–fluid interface of the lid-driven cavity at Re = 100 and Gr = 20,000 in all three geometrical configurations for forced and mixed convection is shown in Fig. 6. From Fig. 6, it is observed that the interface temperature in the case of forward step with mixed convection is lower when compared with that of the temperatures obtained in all other geometrical configurations. The reason for this is because; in the case of forward step, the step is present in the direction of fluid motion. The fluid inside the cavity undergoes

Fig. 6 Temperature distribution along the solid–fluid interface of the lid-driven cavity in the case of pure water at Re = 100 and Gr = 20,000 in all three geometrical configurations for forced and mixed convection
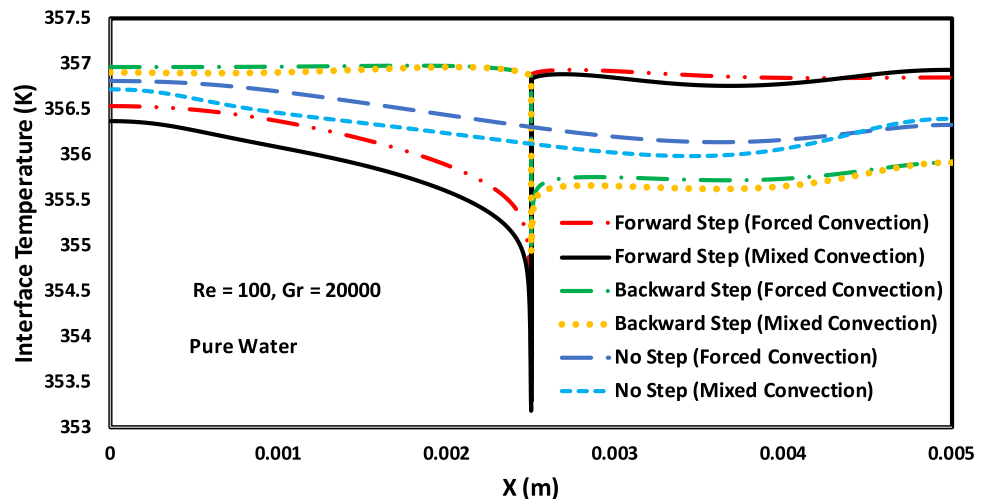
swirling motion due to the movement of the upper / top lid. This moving fluid should climb the step present in its direction of motion thereby causing disturbed local fluid movement due to hitting of the fluid with the step height. This disturbed local movement of fluid will not happen in backward and no step cases. In the case of backward step, the swirling fluid will get down the step in a smooth flow manner as the step is present in the downward direction of the flow. Moreover, at Re = 100, for a particular geometrical configuration, there is a difference between the interface temperatures obtained in the case of forced and mixed convection. This is because; as explained in Figs. 4 and 5, at lower values of Re, domination of forced currents on natural fluid movement is not significant and hence there will be a difference.

7.4 Effect of convection type and Grashof number

Average Nusselt number at different Reynolds number for forced and mixed convection types of pure water in forward step at different Grashof numbers is shown in Fig. 7. From Fig. 7, it is observed that the values of Nu_{avg} obtained in the case of mixed convection with Gr = 20,000 are higher when compared to other cases. The reason for this is because; for a particular heat transfer fluid with constant low temperature (T_l) applied to the moving lid, increment in the Grashof number results in the increase of high temperature (T_h) applied to the bottom wall under the solid region. This results in the increment of ΔT ($T_h - T_l$). This higher ΔT leads to buoyancy effect that results in the natural movement of fluid caused due to difference in the densities of hot and cold fluids along with the bulk fluid movement caused by external forced that is by moving lid. This results in the phenomena of mixed convection to dominate forced convection. Moreover, at lower Grashof numbers (Gr = 5000), the difference between mixed and forced convection is very small. This is because of low T_h value at lower Gr. Furthermore, as Reynolds number

increases, the difference between forced and mixed convection heat transfer decreases for a particular Gr number. This shows that at higher values of Re, the fluid motion is purely caused by means of external force exerted by moving the lid (by the movement of the lid) and buoyancy effect has very minimal impact on the fluid motion. This is because; the forced currents dominate the tendency of natural movement of the fluid caused due to difference in local fluid densities which in turn is due to difference in local temperatures. At lower values of Re, domination of forced currents on natural fluid movement is not significant and hence there will be a difference. For Re = 100 and Gr = 20,000, Nu_{avg} value of mixed convection is 24% higher than that of forced convection.

7.5 Effect of thermal conductivity model

Thermal conductivity of Al_2O_3/water nanofluid at different volume concentrations of nanoparticles dispersed in pure water is shown in Fig. 8 for various thermal conductivity models as given in Table 2. Reference [6–12] represents the thermal conductivity models without consideration of Brownian motion. Whereas, Reference [13–16] represents the thermal conductivity models considering both the Brownian motion and aggregation effects. From Fig. 8, it is clearly understood that Xuan et al. [13] as well as Patel et al. [14] models exhibits higher thermal conductivity when compared with all other models especially at higher volume concentration of nanoparticles. This is because, it considers the micro-convection phenomena that has three contributions for heat flow through the nanofluids. That are, conduction through fluid, conduction through solid and advection because of the Brownian motion of the particles as well as aggregation. The classical thermal conductivity models of Maxwell [6], Bruggeman [7], Hamilton and Crosser [8], as well as Lu and Lin [9], Chon et al. [10], Chandrasekar et al. [11], Dong and Chen [16] exhibits similar thermal conductivity values. From Fig. 8, it is observed

Fig. 7 Average Nusselt number at different Reynolds number for forced and mixed convection types of pure water in forward step at different Grashof numbers
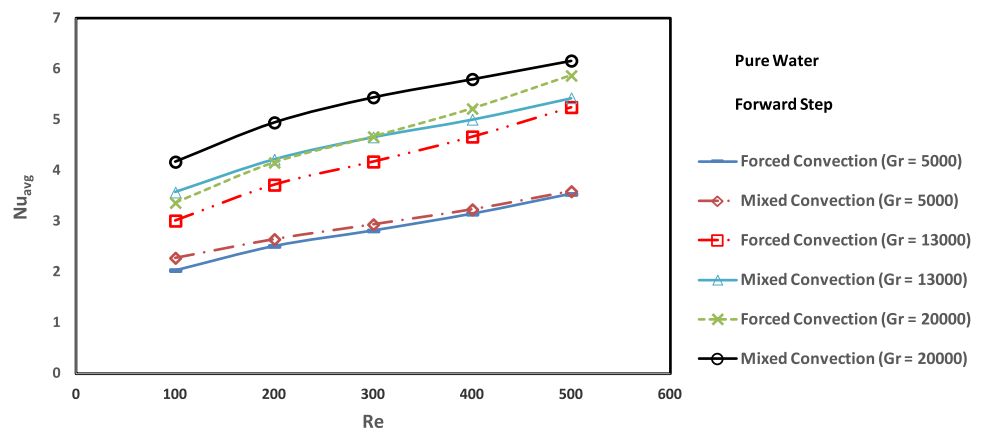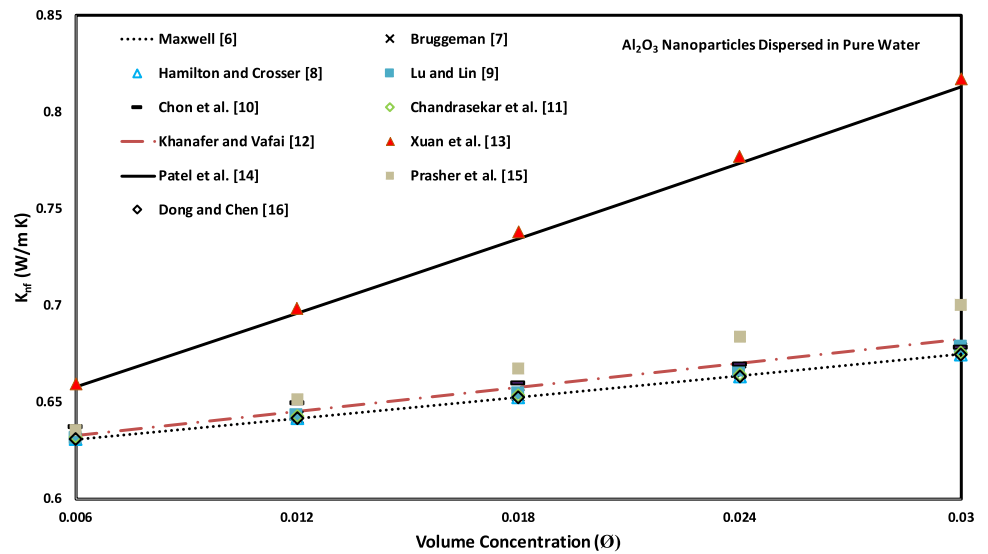
Fig. 8 Thermal conductivity of Al_2O_3/water nanofluid at different volume concentrations of nanoparticles dispersed in pure water


that Patel et al. [14] model results in 20.56% higher thermal conductivity value for 3 vol.% Al_2O_3/water nanofluid in comparison with the lowest thermal conductivity value of Dong and Chen [16] obtained in the present study. The use of micro-convection phenomena based thermal conductivity models will result in higher values of thermal conductivity when compared with other models. Adopting these micro-convection based thermal conductivity models in numerical studies on heat transfer evaluation may also lead to obtain closer results in comparison with experimental data giving rise to very minimal deviation.

7.6 Effect of volume concentration

Average Nusselt number values of different volume concentrations of nanofluid at various Reynolds number for forward step under mixed convection at Gr = 20,000 is shown in Fig. 9. From Fig. 9, it is observed that the Nu_{avg} values of 3 vol.% Al_2O_3/water nanofluid is higher when compared to that of other heat transfer fluids.

This is because of its higher thermal conductivity value when compared with pure water, 1 vol.% Al_2O_3 and 2 vol.% Al_2O_3/water nanofluids. At Re = 500, 3 vol.% Al_2O_3/water nanofluid enhances the heat transfer performance by 23.63% in comparison with that of pure water for mixed convection with Gr = 20,000 in forward step. Whereas,

Fig. 9 Average Nusselt number values of different volume concentrations of nanofluid at different Reynolds number for forward step under mixed convection at Gr = 20,000
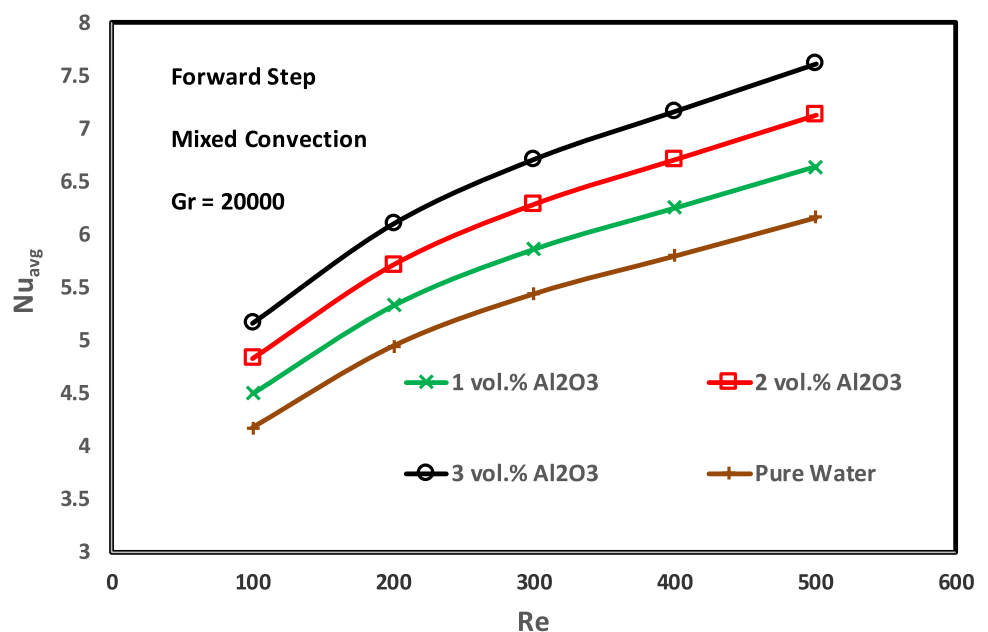
1 vol.% and 2 vol.% Al_2O_3/water nanofluid shows an enhancement of 7.8% and 15.7%, respectively. Moreover, as Re increases, the Nu_{avg} value also increases for a particular heat transfer fluid. This is because of increase in the velocity of the fluid which in turn is due to increase in the velocity of moving lid.

8 Conclusion

Two-dimensional conjugate heat transfer performance of stepped lid-driven cavity was numerically investigated in the present study under forced and mixed convection in laminar regime. Pure water and Aluminium oxide (Al_2O_3)/water nanofluid with $D_p = 30$ nm and 1 vol.%, 2 vol.% and 3 vol.% concentrations were considered. All the numerical simulations were performed by considering brownian motion based effective thermal conductivity evaluation in homogeneous heat transfer model of ANSYS FLUENT. The effect of various parameters such as Reynolds number, Grashof number, geometrical configuration, convection types are comprehensively investigated and presented. The following conclusions are made from the present study.

- At lower values of Re, domination of forced currents on natural fluid movement is not significant and hence there will be a difference in the heat transfer performance between forced and mixed convection. For Re = 100 and Gr = 20,000, Nu_{avg} value of mixed convection is 24% higher than that of forced convection.
- For higher Re values, no much difference in Nu_{avg} is observed between forced and mixed convection. This is because of significant domination of forced currents on natural fluid movement.
- Out of all the three configurations, at Re = 100, forward step with mixed convection gives higher heat transfer performance as the obtained interface temperature is lower than all other cases.
- The effective thermal conductivity of Al_2O_3/water nanofluid evaluated by considering the brownian motion of nanoparticles with Patel et al. [14] results in 20.56% higher value for 3 vol.% Al_2O_3/water nanofluid in comparison with the lowest thermal conductivity value of Dong and Chen [16] obtained in the present study showing the importance and considering requirement of brownian motion in nanofluid heat transfer.
- At Re = 500, 3 vol.% Al_2O_3/water nanofluid enhances the heat transfer performance by 23.63% in comparison with that of pure water for mixed convection with Gr = 20,000 in forward step.

The present work will be benefited to the field of electronics cooling providing no possibility for leakage of working fluid as a result of closed system.

References

1. Manova S, Asirvatham LG, Nimmagadda R, Bose JR, Wongwises S (2020) Cooling of high heat flux electronic devices using ultra-thin multiport minichannel thermosyphon. Appl Therm Eng 169:114669. https://doi.org/10.1016/j.applthermaleng.2019.114669
2. Manova S, Asirvatham LG, Nimmagadda R, Bose JR, Wongwises S (2020) Feasibility of using multiport minichannel as thermosyphon for cooling of miniaturized electronic devices. Heat Transfer. https://doi.org/10.1002/htj.21855
3. Nimmagadda R, Reuven R, Asirvatham LG, Wongwises S (2020) Thermal management of electronic devices using gold and carbon nanofluids in a Lid-Driven square cavity under the effect of variety of magnetic fields. IEEE Trans Compon Packaging Manuf Technol. https://doi.org/10.1109/TCPMT.2020.3008786
4. Returi MC, Konijeti R, Dasore A (2019) Heat transfer enhancement using hybrid nanofluids in spiral plate heat exchangers. Heat Transf Asian Res 48(7):3128–3143. https://doi.org/10.1002/htj.21534
5. Konda, R J, P N, R M, Konijeti R, Dasore A (2019) Effect of non-uniform heat source/sink on MHD boundary layer flow and melting heat transfer of Williamson nanofluid in porous medium. Multidiscipl Model Mater Struct. https://doi.org/10.1108/MMMS-01-2018-0011
6. Maxwell JC (1873) A treatise on electricity and magnetism, vol 1. Clarendon Press, Oxford
7. Bruggeman VD (1935) Berechnung verschiedener physikalischer Konstanten von heterogenen Substanzen. I. Dielektrizitätskonstanten und Leitfähigkeiten der Mischkörper aus isotropen Substanzen. Ann Phys 416(7):636–664. https://doi.org/10.1002/andp.19354160705
8. Hamilton RL, Crosser OK (1962) Thermal conductivity of heterogeneous two-component systems. Ind Eng Chem Fundam 1(3):187–191. https://doi.org/10.1021/i160003a005

9. Lu SY, Lin HC (1996) Effective conductivity of composites containing aligned spheroidal inclusions of finite conductivity. J Appl Phys 79(9):6761–6769. https://doi.org/10.1063/1.361498

10. Chon CH, Kihm KD, Lee SP, Choi SU (2005) Empirical correlation finding the role of temperature and particle size for nanofluid (Al_2O_3) thermal conductivity enhancement. Appl Phys Lett 87(15):153107. https://doi.org/10.1063/1.2093936

11. Chandrasekar M, Suresh S, Bose AC (2010) Experimental investigations and theoretical determination of thermal conductivity and viscosity of Al_2O_3 nanofluid. Exp Thermal Fluid Sci 34(2):210–216. https://doi.org/10.1016/j.expthermflusci.2009.10.022

12. Khanafer K, Vafai K (2011) A critical synthesis of thermophysical characteristics of nanofluids. Int J Heat Mass Transf 54(19–20):4410–4428. https://doi.org/10.1016/j.ijheatmasstransfer.2011.04.048

13. Xuan Y, Li Q, Hu W (2003) Aggregation structure and thermal conductivity of nanofluids. AIChE J 49(4):1038–1043. https://doi.org/10.1002/aic.690490420

14. Patel, H. E., Anoop, K. B., Sundararajan, T., & Das, S. K. (2006) A micro-convection model for thermal conductivity of nanofluids. In *International Heat Transfer Conference 13*. Begel House Inc. DOI: https://doi.org/10.1615/IHTC13.p8.240

15. Prasher R, Bhattacharya P, Phelan PE (2005) Thermal conductivity of nanoscale colloidal solutions (nanofluids). Phys Rev Lett 94(2):025901. https://doi.org/10.1103/PhysRevLett.94.025901

16. Dong S, Chen X (2017) An improved model for thermal conductivity of nanofluids with effects of particle size and Brownian motion. J Therm Anal Calorim 129(2):1255–1263. https://doi.org/10.1007/s10973-017-6256-x

17. Goudarzi S, Shekaramiz M, Omidvar A, Golab E, Karimipour A, Karimipour A (2020) Nanoparticles migration due to thermophoresis and Brownian motion and its impact on Ag-MgO/Water hybrid nanofluid natural convection. Powder Technol 375:493–503. https://doi.org/10.1016/j.powtec.2020.07.115

18. Abdelmalek Z, Hussain A, Bilal S, Sherif ESM, Thounthong P (2020) Brownian motion and thermophoretic diffusion influence on thermophysical aspects of electrically conducting viscoinelastic nanofluid flow over a stretched surface. J Market Res 9(5):11948–11957. https://doi.org/10.1016/j.jmrt.2020.08.014

19. Harish R, Sivakumar R (2021) Effects of nanoparticle dispersion on turbulent mixed convection flows in cubical enclosure considering Brownian motion and thermophoresis. Powder Technol 378:303–316. https://doi.org/10.1016/j.powtec.2020.09.054

20. Lin Y, Jiang Y (2018) Effects of Brownian motion and thermophoresis on nanofluids in a rotating circular groove: A numerical simulation. Int J Heat Mass Transf 123:569–582. https://doi.org/10.1016/j.ijheatmasstransfer.2018.02.103

21. Gibanov NS, Sheremet MA, Oztop HF, Nusier OK (2017) Convective heat transfer of ferrofluid in a lid-driven cavity with a heat-conducting solid backward step under the effect of a variable magnetic field. Numer Heat Transf, Part A: Appl 72(1):54–67. https://doi.org/10.1080/10407782.2017.1353377

22. Gibanov NS, Sheremet MA, Oztop HF, Al-Salem K (2017) Convective heat transfer in a lid-driven cavity with a heat-conducting solid backward step under the effect of buoyancy force. Int J Heat Mass Transf 112:158–168. https://doi.org/10.1016/j.ijheatmasstransfer.2017.04.102

23. Al-Amiri A, Khanafer K, Bull J, Pop I (2007) Effect of sinusoidal wavy bottom surface on mixed convection heat transfer in a lid-driven cavity. Int J Heat Mass Transf 50(9–10):1771–1780. https://doi.org/10.1016/j.ijheatmasstransfer.2006.10.008

24. Khanafer K, Aithal SM (2013) Laminar mixed convection flow and heat transfer characteristics in a lid driven cavity with a circular cylinder. Int J Heat Mass Transf 66:200–209. https://doi.org/10.1016/j.ijheatmasstransfer.2013.07.023

25. Gangawane KM (2017) Computational analysis of mixed convection heat transfer characteristics in lid-driven cavity containing triangular block with constant heat flux: Effect of Prandtl and Grashof numbers. Int J Heat Mass Transf 105:34–57. https://doi.org/10.1016/j.ijheatmasstransfer.2016.09.061

26. Khan ZH, Khan WA, Hamid M, Liu H (2020) Finite element analysis of hybrid nanofluid flow and heat transfer in a split lid-driven square cavity with Y-shaped obstacle. Phys Fluids 32(9):093609. https://doi.org/10.1063/5.0021638

27. Valizadeh Ardalan M, Alizadeh R, Fattahi A, Adelian Rasi N, Doranehgard MH, Karimi N (2020) Analysis of unsteady mixed convection of Cu–water nanofluid in an oscillatory, lid-driven enclosure using lattice Boltzmann method. J Therm Anal Calorim. https://doi.org/10.1007/s10973-020-09789-3

28. Pak BC, Cho YI (1998) Hydrodynamic and heat transfer study of dispersed fluids with submicron metallic oxide particles. Exp Heat Transf Int J 11(2):151–170. https://doi.org/10.1080/08916159808946559

29. Xuan Y, Roetzel W (2000) Conceptions for heat transfer correlation of nanofluids. Int J Heat Mass Transf 43(19):3701–3707. https://doi.org/10.1016/S0017-9310(99)00369-5

30. Nimmagadda R (2018) Buoyancy-driven heat transfer performance of pure and hybrid nanofluids in minienclosure. J Thermophys Heat Transfer 32(3):570–579. https://doi.org/10.2514/1.T5324

31. Brinkman HC (1952) The viscosity of concentrated suspensions and solutions. J Chem Phys 20(4):571–571. https://doi.org/10.1063/1.1700493

32. Ho CJ, Wei LC, Li ZW (2010) An experimental investigation of forced convective cooling performance of a microchannel heat sink with Al_2O_3 nanofluid. Appl Therm Eng 30(2–3):96–103. https://doi.org/10.1016/j.applthermaleng.2009.07.003

33. Albojamal A, Vafai K (2017) Analysis of single phase, discrete and mixture models, in predicting nanofluid transport. Int J Heat Mass Transf 114:225–237. https://doi.org/10.1016/j.ijheatmasstransfer.2017.06.030

34. Bianco V, Chiacchio F, Manca O, Nardini S (2009) Numerical investigation of nanofluids forced convection in circular tubes. Appl Therm Eng 29(17–18):3632–3642. https://doi.org/10.1016/j.applthermaleng.2009.06.019

35. Nimmagadda R, Venkatasubbaiah K (2015) Conjugate heat transfer analysis of micro-channel using novel hybrid nanofluids (Al_2O_3+Ag/Water). Eur J Mech-B/Fluids 52:19–27. https://doi.org/10.1016/j.euromechflu.2015.01.007

36. Ghia UKNG, Ghia KN, Shin CT (1982) High-Re solutions for incompressible flow using the Navier-Stokes equations and a multigrid method. J Comput Phys 48(3):387–411

37. Mohammed S, Reis T (2017) Using the lid-driven cavity flow to validate moment-based boundary conditions for the lattice Boltzmann equation. Archive of Mech Eng 64(1):57–74. https://doi.org/10.1515/meceng-2017-0004

38. Lamraoui H, Mansouri K, Saci R (2019) Numerical investigation on fluid dynamic and thermal behavior of a non-Newtonian Al_2O_3–water nanofluid flow in a confined impinging slot jet. J Nonnewton Fluid Mech 265:11–27. https://doi.org/10.1016/j.jnnfm.2018.12.011

39. Abhijith MS, Venkatasubbaiah K (2020) Numerical investigation of jet impingement flows with different nanofluids in a mini channel using Eulerian-Eulerian two-phase method. Thermal Sci Eng Progress. https://doi.org/10.1016/j.tsep.2020.100585